Solar Energy 258 (2023) 304–318

Contents lists available at ScienceDirect

Solar Energy

journal homepage: www.elsevier.com/locate/solener

Comprehensive thermoeconomic study of a new solar thermosyphon-assisted multigeneration system

Rasoul Najafi Anamaq [a], Leyla Khani [a], Mousa Mohammadpourfard [b,a,*], Saeed Zeinali Heris [a], Gülden Gökçen Akkurt [b]

[a] Faculty of Chemical and Petroleum Engineering, University of Tabriz, Tabriz, Iran
[b] Department of Energy Systems Engineering, Izmir Institute of Technology, Izmir, Turkey

ARTICLE INFO

Keywords:
Exergy
Thermosyphon cooling
Multigeneration
Exergoeconomic
Solar
Desalination

ABSTRACT

Nowadays, due to the global energy crisis, limited reservoirs of fossil fuels, and their negative environmental effects, the use of renewable energy sources and multigeneration systems have become good alternatives for conventional thermodynamic systems. One of these resources, whose technology has developed rapidly in recent years, is the use of solar energy for the simultaneous generation of various products. Therefore, in this research, a multigeneration system with several subsystems is introduced. The proposed system includes a solar energy collector to receive thermal energy, two thermal energy storage tanks, an organic Rankine cycle, and a Kalina cycle to generate electricity, a multi-effect distillation unit to produce fresh water, an electrolyzer to produce hydrogen, as well as heat recovery for hot water and hot air generation. In this multigeneration system, the cooling unit is designed with the help of a thermosyphon. The performance of the proposed system is studied from energy, exergy, environmental, and exergoeconomic viewpoints using Aspen HYSYS and EES software. The obtained results show that due to the addition of the thermosyphon unit to the refrigeration system, the exergy efficiency increases from 55.62% to 70.26%. As a result of this combination, the performance of the whole system is improved and the amount of costs are reduced. In addition, the parabolic collector system has the highest exergy destruction ratio, 39%, among the subsystems. Furthermore, the results of the exergoeconomic analysis indicate that the PEM water heater with 33.3% and the ejector with 22.7% own the highest cost destruction rates.

1. Introduction

Sustainable development can be defined as a state of human development in which the use of energy resources is conditional on the absence of adverse effects on the environment and the needs of future generations. The relationship between energy, environment, and sustainable development is in fact similar to three vertices of an equilateral triangle, and there should be a balance between these items in designing thermodynamic systems. Today, fossil fuels provide most of the total energy production capacity, but their utilization leads to environmental pollution, and cause climate change, global warming, acid rains, deforestation, and health problems. It is also predicted that with the current trend of pollution emission, the health of human being and other living organisms will be in danger [1]. Hence, strict environmental laws have been enacted and considerable funds are allocated for research in the field of renewable energy sources, optimum energy conversion methods, and maximum use of fuels' chemical energy [2].

The share of renewable energy sources in the global energy market is increasing due to their numerous advantages like less pollution, enhanced health condition, more stability and durability, lower costs, economic benefits, and environmental friendliness. Among renewable energies, solar energy is the most popular due to its high potential, high availability, and vast dispersion. It is the primary source of all energy types of the earth [3].

Furthermore, special attention should be paid to heat and material recovery from primary thermodynamic systems as useful inputs for other subsystems to generate more products and maximize the efficiency of energy systems. These systems, called combined or multigeneration systems, have several advantages such as high efficiency, better reliability, low cost, and reduced emission [4].

The urgent need for freshwater production, especially in hot arid areas has always been one of the most important issues in the economical and industrial fields. Therefore, the use of seawater

* Corresponding author at: Faculty of Chemical and Petroleum Engineering, University of Tabriz, Tabriz, Iran.
E-mail addresses: mohammadpour@tabrizu.ac.ir, mousamohammadpourfard@iyte.edu.tr (M. Mohammadpourfard).

https://doi.org/10.1016/j.solener.2023.05.005
Received 24 January 2023; Received in revised form 2 April 2023; Accepted 3 May 2023
Available online 12 May 2023

Nomenclature

A	Area $[m^2]$
C	Cost ($)
c	Specific cost ($/MJ)
E	Energy,[kJ]
$\dot{E}$	Energy flow rate, [kW]
ex	Specific exergy, [kJ/kg]
e^{PH}	Physical exergy, [kJ/kg]
e^{CH}	Chemical exergy,[kJ/kg]
$\dot{E}x$	Exergy, [kW]
$\dot{E}x_D$	Exergy destruction rate, [kW]
F	Faraday constant, [C/mol]
G	Gibbs energy
h	Specific enthalpy, [kJ/kg]
I_d	Direct normal irradiation, $[W/m^2]$
J	Current density, $[A/m^2]$
J_o	Exchange current density, $[A/m^2]$
J_i^{ref}	Pre-exponential constant,$[A/m^2]$
m	Mass, [kg]
$\dot{m}$	Mass flow rate,[kg\s]
P	Pressure, [kPa]
Q	Heat [kJ]
$\dot{Q}$	Heat flow rate [kW]
R	Universal gas constant,[kJ/mol −K]
s	Specific entropy, [kJ/kgK]
T	Temperature, [K or °C]
$V_{act.a}$	Activation energy for anode, [kJ/mol]
$V_{act.c}$	Activation energy for cathode, [kJ/mol]
$\dot{W}$	Work rate, [kw]
$\dot{Z}$	Capital cost rate,[$/s]
Z	Equipment purchase cost [$]

Greek Letters

η	Energy efficiency
ψ	Exergy efficiency
σ	Stefan-Boltzmann Constant
φ	Operating and maintenance costs
θ	Temperature drop

Subscripts

a	Anode
ar	Air
c	Cathode and cost rate
ch	Chemical
chr	primary charged
chp	Final charged
$chst$	Compressed hydrogen storage tank
cr	Collector receiver
cv	Control Volume
D	Destruction
disf	Discharged
$ejec$	Ejector
en	Energy
ex	Exergy
Elec	Electrolyzer
F	Feed
i	Interest rates
in	Inlet
id	Inside diameter
k	Components
L	Loss
od	Outside diameter
out	Outlet
p	Product
ph	Physical
rad	Radiation
rcv	Receiver
str	Stored
sc	Solar collector
scp	Solar-collecting plates
stL	Heat loss the storage tank
o	Standard state
w	Water
wf	Working fluid

Acronyms

Abs	Absorber
CI	Cost Investment
$Comp$	Compressor
$Cond$	Condenser
COP	Coefficient of performance
CRF	Capital recovery factor
CS	Ejector cooling cycle
$CTST$	Cold temperature storage tank
DC	Drying cycle
DWH	Domestic water heater
Eva	Evaporator
FWST	Freshwater storage tank
FWGS	Freshwater generation subsystem
GEN	Generator
HGCS	Hydrogen generation and compression subsystem
$HTST$	Hot temperature storage tank
HC	Hydrogen compressor
HEX	Heat exchanger
MED	Multi-effect distillation unit
KC	Kalina cycle
KHex	Kalina Heat Exchanger
OM	Operation and Maintenance costs
ORC	Organic Rankine cycle
P	Pump
PEM	Proton exchange membrane
PSC	Parabolic solar collector
PSF	Parabolic solar field
SI	sustainability index
T	Turbine
VLV	Valve

desalination technology can be one of the most effective and useful methods to compensate for potable water shortage. Conventional seawater desalination systems are based on evaporation and distillation mechanisms and need a great amount of energy usually provided by fossil fuels. However, it has been shown that seawater desalination systems can also work with solar energy, which leads to lower cost, less pollution, and higher sustainability.

Researchers have recently gone beyond the one-purpose production system and try to design systems that use waste energy from an upper system to produce more than one product such as electricity, hot water, and valuable materials using primary energy sources.

Ahmadi et al. [5] modeled a trigeneration system for producing cooling, heating, and electrical power, including a gas turbine cycle, a Rankine cycle, an absorption refrigeration system, and an internal water

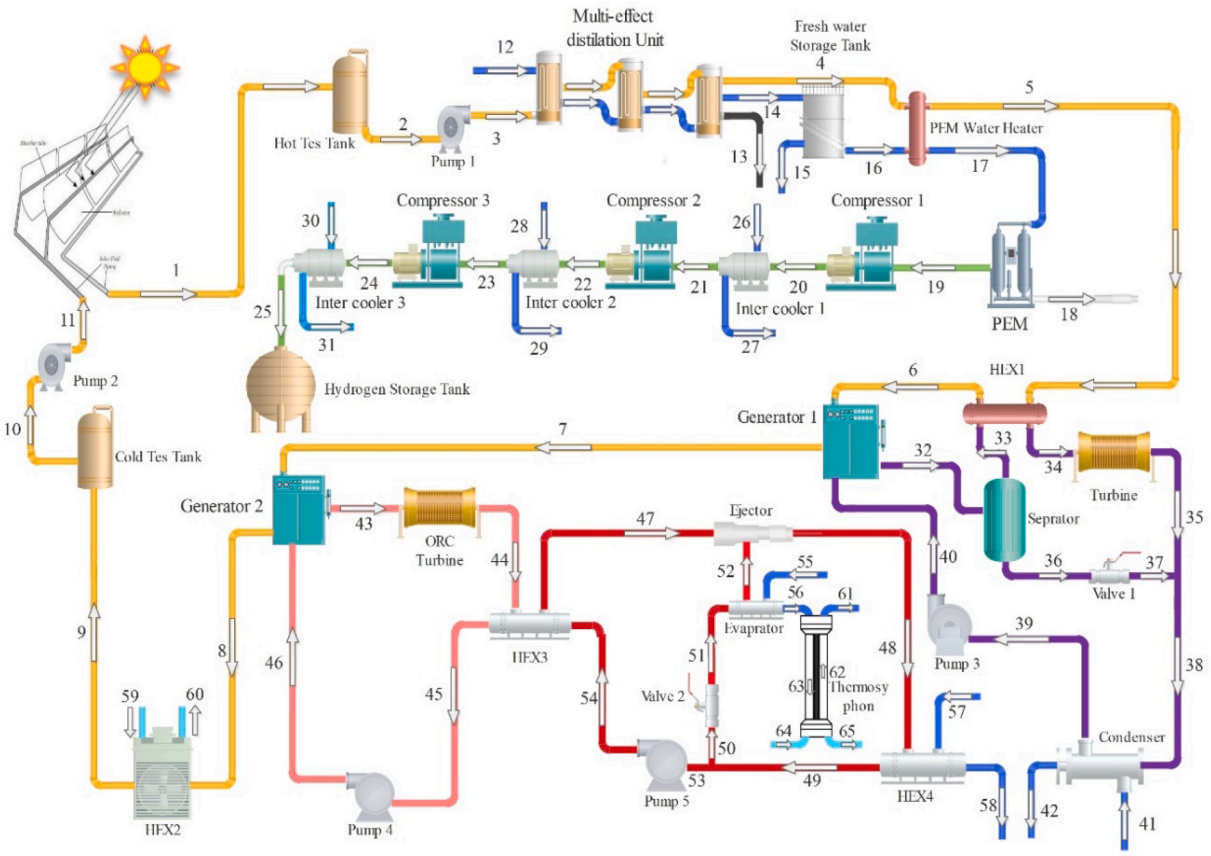

Material	Pipe Color
Water	
Ammonia-Water	
Isobutane	
Hydrogen	
R113	
Oxygen	
Terminol66	
Air	
Methanol	

Fig. 1. The proposed solar-based electrical power, cooling, heating, hydrogen, dry air, and freshwater multigeneration system.

heater. They analyzed the energy, exergy, and environmental performances of their system. Their parametric analyses revealed that the trigeneration system's energy efficiency and environmental effect are highly influenced by the compressor pressure ratio, gas turbine input temperature, and isentropic efficiency of the gas turbine. Additionally, lowering the mass flow rate through the combustion chamber and raising the turbine input temperature reduce the cost of environmental effect. Murat oztürk et al. [6] studied a cogeneration system for electrical power, heating, cooling, and hydrogen production and presented an exergy efficiency of 57.35% and the highest exergy destruction rate in solar collectors. Leiva-Illanes et al. [7] showed that solar-based multigeneration systems are more economically efficient than related single, hybrid, and trigeneration systems because they create lower unit exergy costs per product. Different processes were compared to determine the equipment and processes with the most destruction rate. According to the results, the best process was the multigeneration process, which reduced the cost of electricity, water, cooling, and heating by 6.8%, 59.2%, 45.6%, and 32.2%, respectively. Chen et al. [8] evaluated a powerplant combined with solar energy with electricity and cooling outputs. In this study, the analysis of energy, and exergy operation is

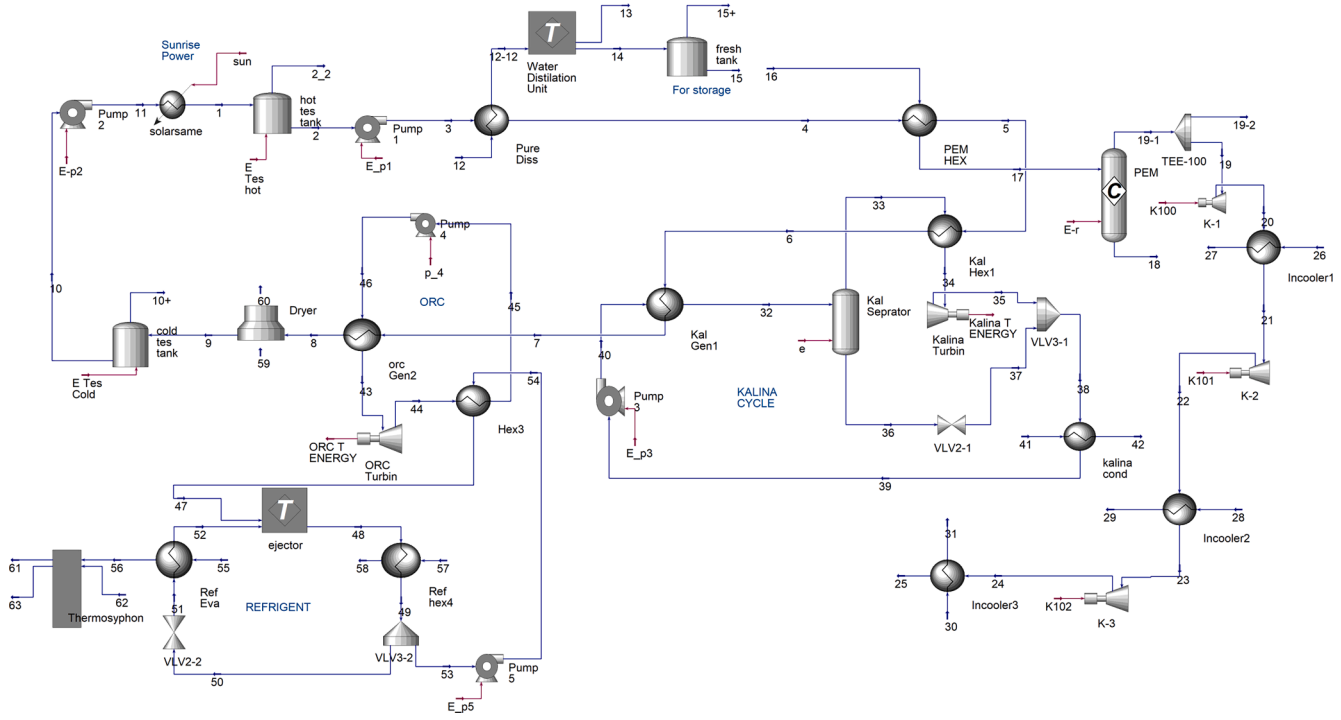

Fig. 2. Simulation flowsheet of the proposed system in Aspen HYSYS software.

performed, and the effect of key parameters on the system performance was investigated. The energy and exergy efficiencies of the system were 70.35% and 45.52%, respectively with a renewable energy ratio of 18.1%. Cesar and Koch [9] studied the performance of a new system with variations in the effective parameters such as light intensity, wind intensity, and ambient temperature. They calculated the energy and exergy efficiencies of the system as 73.3% and 30.6%, respectively, while the most exergy destruction was in the solar system. Nejat et al. [10] designed a hybrid powerplant based on parabolic solar collectors. Their evaluation results showed that the energy and exergy efficiencies of the whole system were 59.34% and 56.51%, respectively. Murat et al. [11] evaluated a new hybrid solar-based system with molten salt energy storage for the production of fresh water and electricity. The molten salt in the hot storage tank compensated for the lack of energy when the normal direct radiation level was not sufficient enough. The electricity generation capacity of the integrated system was obtained as 13.5 MW. Also, 3958 tons/day fresh water was produced in the multistage flash distillation unit. Solar receiver and steam generator represented 73% of the overall exergy destruction rate. Taohi et al. [12] investigated the performance of a cooling system for refrigeration applications. They concluded that number of fans for air circulation over thermosyphon evaporator in the refrigerated chamber affected the interior temperature. Casalas and Dinser [13] analyzed a new powerplant to produce hydrogen and ammonia. It was suggested to use a solar-powered system that included a fuel cell component to synthesize ammonia in a sustainable manner while consuming just 60% of the original amount of electricity. Hosseinnia et al. [14] investigated optimal configuration of an intelligent parking lot and hydrogen, heat and power production microgrid with a reliability-constrained optimization model. The suggested model concurrently maximized the performance of emissions and economic expenses. All uncertainties were generated using a combination of the Latin hypercube sampling process and the K-means clustering algorithm. Hence, the total emission and economic costs of the microgrid was reduced to 4.01% and 1.72%, respectively. Solar desalination is a process to convert saline water into potable water by the application of solar energy. A heat exchanger is an important device used for heat transfer applications. The present study shows the application of heat exchangers to enhance the distillate output of solar desalination systems and shows the combination of the solar desalination system with a PTC and heat exchanger improved the solar desalination system's performance compared with the passive solar desalination system [15]. Nabat et al's combination of a conventional combustion chamber, a cavity receiver, high-temperature molten salt, and thermal energy storage included a concentrated solar power system with the heliostat field. The system generated roughly 53.9 MW of electrical power and 55 kg/s of residential hot water during periods of peak demand [16]. The round-trip energy and exergy efficiencies of the system were estimated as 54.05% and 46.51%, respectively. Applying the suggested concept to the instance of San Diego using actual hourly data produced an annual production of green electricity of around 25 GWh and averted the release of more than 5100 tons of CO2 from the atmosphere. According to their economic study, the planned system in this city had a payback period of 2.42 years and an overall profit of 137.4 M$. Ammar H. Elsheikh et al. [17] presented a new compact design of a vertical water distillation tower based on solar stills. The water yield and thermal, exergic, and economic features of the tower were investigated and analyzed. A powerful artificial intelligence tool was integrated with the optimizer to predict the water yield and temperature of the established tower. The developed system provides considerable improvement compared with conventional designs of solar stills.

According to the above-mentioned literature review, various papers have been published on renewable energy-based combined systems. However, it seems that more novelty and combination scenarios are necessary to assess the performance of different unit in integrated systems and design new multigeneration systems for different conditions and purposes. In this regard, thermosyphon-assisted refrigeration units are one of interesting subsystems that can recover waste heat of an upper system leading to higher efficiency. Thermosyphon is a heat transfer device in which gravity is used to flow the condensed liquid towards the evaporating part and its benefits are simple geometrical building, low installation and maintenance cost, no moving part, compatibility for design in different dimensions, and various working fluids. These advantages make thermosyphon more reliable and economical than other heat transfer devices and have promoted its utilization in a wide range of

Table 1
Input parameters for the system modeling [20–21].

Parameters	Values
Ambient temperature,T_0	25 °C
Ambient pressure,P_0	101.3 kPa
Solar radiation intensity,G	750 W/m^2
Outside diameter of collector tube,D_{od}	0.018 m
Inside diameter of collector tube,D_{id}	0.014 m
Solar collector area,A_{sc}	395 m^2
Number of solar-collecting plates,N_{scp}	132
Pump isentropic efficiency,η_P	0.80
Kalina turbine isentropic efficiency,η_{KT}	0.80
ORC turbine isentropic efficiency,η_{orc-T}	0.75
Pinch point temperature of generator 1,$T_{pp-gen1}$	18 °C
Ejector entrainment ratio,φ_{eject}	0.4468
Energetic coefficient of performance,COP_{en}	1.841
Exergetic coefficient of performance,COP_{ex}	0.627
Fresh water salinity	450 ppm
Seawater salinity	35,000 ppm
Annual operating hour, N	7000
Operating and maintenance costs, φ	1.06
Interest rates, i	0.15

engineering applications such as reboilers, heaters, and cooling systems [18]. Hence, in this research, a novel solar energy-based multi-generation system consisting of a parabolic solar energy collector, thermal energy storage tanks, a multi-effect distillation unit, a Kalina cycle, a hydrogen production section, an air dryer, a thermosyphon-assisted refrigeration cycle and an organic Rankine cycle is proposed to generate electricity, heating, cooling, freshwater, drying air, and hydrogen. Solar collector can be a good option for combined systems, since it has the low life cycle cost and high commercialization [19]. In the design step, special attention is paid to maximum heat recovery among the integrated subsystems, so the efficiency of the multi-generation system increases, the energy waste is decreased, and lower amount of external energy becomes necessary. Then, first and second laws of thermodynamics along with exergoeconomic relationships and auxiliary equations are applied to each component and the whole system at the steady state, using Aspen HYSYS software. Due to the importance of environmental issues, sustainability index is used to examine the environmental impact of the proposed system. The sustainability index can relate environmental performance of a system to its exergy efficiency. After that, the results obtained from a solar energy-based multigeneration system consisting thermosyphon-assisted refrigeration unit as a novelty of this system combination are presented and explained in detail.

2. System description

The proposed solar-based electrical power, heating, cooling, hydrogen, drying air, and freshwater multigeneration system is shown in Fig. 1. The integrated subsystems are solar energy collecting cycle with thermal energy storage tanks, multi-effect distillation unit, hydrogen production unit, Kalina cycle, organic Rankine cycle, air dryer, and thermosyphon-assisted cooling cycle. The simulation flowsheet of the proposed system in Aspen HYSYS software is depicted in Fig. 2.

The system performance can be explained as follows:

- The solar energy cycle works from stream 1 to stream 11. The working fluid, terminol 66, receives solar energy in the parabolic collector and goes to the hot thermal energy storage tank to set in a suitable temperature. Then, it flows to the bottoming subsystems to provide their necessary energy and finally comes back to the solar collector after passing cold thermal energy storage tank and Pump 2.
- A multi-effect distillation unit is used to produce freshwater. Seawater is the input of this unit and is heated by solar energy at each stage. The outlets of the desalination unit are potable water, which is stored in freshwater storage tank, and brine, which is ejected to the environment. A part of the produced freshwater is used to generate hydrogen, and the remainder is considered for domestic utilization.
- A part of freshwater from the desalination unit gets hot in the PEM (Proton exchange membrane) water heater using solar energy and then, enters the PEM. In the electrolyzer, water is splitted to hydrogen and oxygen. The generated hydrogen is stored at proper condition after passing through three compressors and their related intercoolers, while the oxygen is emitted to the ambient.
- Kalina cycle receives heat from solar energy in HEX1 (Heat Exchanger) and Generator1, and produces electrical power. The ammonia-water solution is heated in Generator1 and sent to the separator to be divided into two streams: vapor section as stream 33 (with higher concentration of ammonia) gets more heat in HEX1 and then generates power by expanding in the turbine, and liquid section as stream 36 (with lower concentration of ammonia), whose pressure decrease while passing through Valve1. The outlet of the turbine mixes with that of Valve1 and enters the condenser to emit heat to the cooling water. The resultant stream with lower pressure and temperature gets pumped to Generator1 to complete the cycle.
- The organic Rankine cycle is composed of generator2, ORC (Organic Rankine cycle) turbine, HEX3, and pump4. Its working fluid, R113, receives solar energy in generator2 and turns into pressurized saturated steam. Then, it is sent to ORC turbine where it expands and produces electrical power. ORC turbine outlet stream becomes saturated liquid at HEX3. Finally, R113 liquid enters pump3 to reach high pressure and complete the ORC cycle.
- The thermosyphon-assisted ejector refrigeration cycle works with the excess heat of ORC released in the HEX3. The high-pressure primary fluid from HEX3 and the low-pressure secondary fluid from the evaporator enter the ejector. Then, the mixed stream flows to HEX4 and gets cooled. The condensed liquid is divided in two parts. Stream 53 is sent back to HEX3 through Pump5. Stream 50 passes Valve2 and then, is used to generate cooling in the evaporator and thermosyphon. After that, it flows to the ejector.
- The working fluid of the solar cycle enters HEX2 as air dryer to produce drying air. Next, it is sent to cold thermal storage tank and Pump2 to complete the solar cycle.

3. System modeling

In this section, a comprehensive thermodynamic and exergoeconomic analysis is performed to evaluate the system performance under the following assumptions [20–21]:

- The system operates under steady-state condition.
- Pressure drop of all equipment is ignored.
- Kinetic and potential energy and exergy terms are negligible.
- Components heat loss to the environment is ignored.

Also, the necessary input data for the system simulation are listed in Table 1 [20–21].

The mass and energy balance equations for a component as a steady-state control volume can be defined as following:

$$\Sigma \dot{m}_{in} = \Sigma \dot{m}_{out} \tag{1}$$

$$\Sigma \dot{m}_{in} h_{in} + \dot{Q}_{cv} = \Sigma \dot{m}_{out} h_{out} + \dot{W}_{cv} \tag{2}$$

The ammonia concentration balance for Kalina cycle can be expressed as:

$$\Sigma \dot{m}_{in} x_{in} = \Sigma \dot{m}_{out} x_{out} \tag{3}$$

Exergy relationship for a component determines the exergy destruction rate due to irreversibilties in a component as below [22]:

$$\Sigma \dot{m}_{in}\, ex_{in} + \dot{E}x_{\dot{Q}} = \Sigma \dot{m}_{out}\, ex_{out} + \dot{E}x_{\dot{W}} + \dot{E}x_D \tag{4}$$

Table 2
Component purchase cost [24–25].

Equipment	Purchase cost
Pump	$Z_P = 1120 \times (\dot{W}_P^{0.8})$
Generator	$Z_{GEN} = 1000 \times (A_{GEN})^{0.65}$
Turbine	$Z_T = 4405 \times (\dot{W}_T)^{0.89}$
Compressor	$Z_{Comp} = \left(\frac{39.5 \times \dot{m}}{0.9 - \eta_{Comp}}\right) \times (P_{out}/P_{in}) \times \ln(P_{out}/P_{in})$
Exchanger	$Z_{Hex} = 516.62 \times (A_{Hex})^{0.65}$
Kalina Heat Exchanger	$Z_{KHex} = 309.14 \times \left(\frac{\dot{Q}_{KHex}}{0.2\Delta T_{KHex}}\right)^{0.85}$
Evaporator	$Z_{Eva} = 309.14 \times (A_{Eva})^{0.85}$
Expansion valve	$Z_{vlv} = 37 \times (\frac{P_{in}}{P_{out}})^{0.68}$
Condenser	$Z_{Cond} = 130 \times (A_{Con}/0.093)^{0.78}$
PEM Electrolyzer	$Z_{PEM} = 1000 \times \dot{W}_{PEM}$
Storage tank	$Z_{str} = 1.15 \times 10^4 \times (\frac{V_{str}}{5})^{0.53}$
Multi-effect distillation unit	$Z_{MED} = 0.3 \times \dot{m}_{MED}$
Parabolic solar collector	$Z_{PSC} = 250 \times A_{PSC}$
Ejector	$Z_{ejec} = 1000 \times 15.96 \times \dot{m}\left(\frac{T_{in} + 273.14}{\frac{P_{in}}{1000}}\right)^{0.5} \times \left(\frac{P_{out}}{1000}\right)^{-0.75}$

In the absence of electrical, magnetic, nuclear, and surface tensions and ignoring kinetic and potential exergies, the exergy of a material stream is the sum of physical and chemical exergy terms:

$$ex = ex_{ch} + ex_{ph} \tag{5}$$

$$ex_{ph} = (h - h_0) - T_0(s - s_0) \tag{6}$$

$$ex_{ch} = \sum_k y_k \bar{e}_k^{ch} + \bar{R}T_0 \sum_k y_k \ln y_k \tag{7}$$

where $\bar{e}^{ch}$ is the standard chemical exergy.

The chemical exergy for the ammonia-water mixture can be calculated as:

$$ex_{ch} = \left(\frac{x}{MW_{NH3}}\right)\bar{e}_{NH3}^{ch} + \left(\frac{1-x}{MW_{water}}\right)\bar{e}_{water}^{ch} \tag{8}$$

Exergoeconomic equation calculates the price of a stream based on its exergy rate, and is expressed as following [23]:

$$\Sigma c_{in}\dot{m}_{in}\, ex_{in} + \Sigma c_q \dot{Q}_{cv} + \dot{Z} = \Sigma c_{out}\dot{m}_{out}\, ex_{out} + \Sigma c_w \dot{W}_{cv} \tag{9}$$

The unit capital cost rate, $\dot{Z}$, is calculated as follows:

$$\dot{Z} = \frac{Z.CRF.\varphi}{N.3600} \tag{10}$$

CRF is the capital recovery factor which is as follows:

$$CRF = \frac{i(1+i)^n}{(1+i)^n - 1} \tag{11}$$

Z is the equipment purchase cost that is listed in Table 2 [24–25].

The necessary data for calculating equipment cost, such as the heat exchanging surface area or stream flow rate, are calculated using ASPEN HYSYS software. Moreover, some components require auxiliary equations to model their performance, which are explained in subsequent sections.

3.1. Parabolic solar collector

The heat transfer rate between ambient air and the parabolic collector is given as [26,27]:

$$\dot{Q}_{solar} = \dot{Q}_h - \dot{Q}_{cr\text{-}loss} = \dot{m}_1 h_1 - \dot{m}_{11} h_{11} = \dot{m}_1 c_{p.1} T_1 - \dot{m}_{11} c_{p.11} T_{11} \tag{12}$$

Here, $\dot{Q}_h$ indicates the rate of heat transfer from the reflector surface of the collector, which can be represented by [27]:

$$\dot{Q}_h = A_{r.PSC} \cdot n \cdot G \cdot \eta_{PSC} \tag{13}$$

$\dot{Q}_{cr.loss}$, the amount of heat loss energy of collector receiver, is calculated as follows [27]:

$$\dot{Q}_{cr.loss} = \dot{Q}_{conv} + \dot{Q}_{rad} = A_{r.PSC}{}^* \left[h_c{}^*(T_{cr} - T_o) + \sigma\varepsilon\left(T_{cr}^4 - T_o^4\right)\right] \tag{14}$$

h_c represents the convective heat transfer coefficient of the air, and is defined by the following equation [11,27]:

$$h_c = 10.45 - \upsilon_{ar} + 10\sqrt{\upsilon_{ar}} \tag{15}$$

here υ_{ar} presents wind speed.

3.2. Thermal energy storage tanks

The calculation of thermal energy storage rate can be described as following [20,27]:

$$\dot{Q}_{ch} = \dot{Q}_{chr} - \dot{Q}_{chp} = M_{st}.C_{p.chr}\left(T_{chr} - T_{chp}\right) \Big/ dt \tag{16}$$

M_{st}, the mass of terminal 66 accumulated during the charge period, is determined by following equation [20,27]:

$$M_{st} = \int_{t_p}^{t_r} m_1 .dt \tag{17}$$

The heat loss from the storage tank is obtained as [20,27]:

$$\dot{Q}_{stL} = \dot{Q}_{chr} - \dot{Q}_{str} = M_{st}C_{p.stL}\left(T_{chr} - T_{str}\right) \Big/ dt \tag{18}$$

In addition, the dissipated heat is calculated as [20,27]:

$$\dot{Q}_{dis} = \dot{Q}_{chr} - \dot{Q}_{disf} = M_{st}{}^* C_{p.dis}\left(T_{chr} - T_{disf}\right) \Big/ dt \tag{19}$$

Where T_{disf} gives us the discharge temperature and calculated the value of c_p for several different temperatures from the following equation [20,27]:

$$c_{p.i} = 1443 + 0.172T_i \,(i = chr,\ stL \text{ and } dis) \tag{20}$$

3.3. Hydrogen production unit

Thermodynamic analysis of the proton exchange membrane electrolyser is described using electrochemical evaluation. The water splitting reaction is as following:

$$H_2O \rightarrow H_2 + \frac{1}{2}O_2 \tag{21}$$

The required energy for this component can be evaluated as [27]:

$$\Delta H = \Delta G + T\Delta S \tag{22}$$

In addition, the molar amount of produced hydrogen is calculated as following [27]:

$$\dot{N}_{H_2.out} = \frac{J}{2F} = \dot{N}_{H_2o.out} (23)$$

The required power for the electrolyzer can be determined from the following equation:

$$\dot{E}_{Elec} = JV \tag{24}$$

Table 3
Design parameters of PEM [28].

Parameter	Value
Operating current density	5000 A/m^2
Anode activation energy . $E_{act.a}$	76kj/kmol
Cathode activation energy,$E_{act.c}$	18 kj/kmol
Water content at the anode membrane,λ_a	14
Water content at the cathode membrane,λ_c	10
Exchange current density of anode,$J_{ref.a}$	1×10^5 A/m^2
Exchange current density of cathode,$J_{ref.c}$	10 A/m^2

Table 4
Energy and exergy efficiency terms for the subsystems.

Sub-system	Energy efficiency	Exergy efficiency
Parabolic collector field	$\eta_{PCF} = \frac{\dot{m}_1(h_1 - h_{11}) - (\dot{W}_{P1} + \dot{W}_{P2})}{\dot{Q}_{solar}}$	$\psi_{PCF} = \frac{\dot{m}_1(ex_1 - ex_{11}) - (\dot{E}x^W_{P1} + \dot{E}x^W_{P2})}{\dot{E}x^Q_{Solar}}$
Fresh water generation subsystem	$\eta_{FWGS} = \frac{\dot{m}_{15}h_{15} + \dot{m}_{16}h_{16}}{\dot{m}_{12}h_{12} + \dot{m}_3(h_3 - h_4)}$	$\psi_{FWGS} = \frac{\dot{m}_{15}ex_{15} + \dot{m}_{16}ex_{16}}{\dot{m}_{12}ex_{12} + \dot{m}_3(ex_3 - ex_4)}$
Hydrogen generation and compression subsystem	$\eta_{HGCS} = \frac{\dot{m}_{25}h_{25}}{\dot{m}_{17}h_{17} + \sum \dot{W}_{HC}}$	$\psi_{HGCS} = \frac{\dot{m}_{25}ex_{25}}{\dot{m}_{17}ex_{17} + \sum \dot{E}x^W_{HC}}$
Kalina cycle	$\eta_{KC} = \frac{\dot{W}_{Tur} + \dot{Q}_{HG\_KC}}{\dot{m}_6(h_6 - h_7)}$	$\psi_{KC} = \frac{\dot{E}x^W_{Tur} + \dot{E}x^Q_{HC\_KC}}{\dot{m}_5(ex_5 - ex_7)}$
Organic Rankine cycle	$\eta_{ORC} = \frac{\dot{W}_{ORC\_T} + \dot{Q}_{HG\_ORC}}{\dot{m}_7(h_7 - h_8)}$	$\psi_{ORC} = \frac{\dot{E}x^W_{ORC\_T} + \dot{E}x^W_{HC\_ORC}}{\dot{m}_7(ex_7 - ex_8)}$
Thermosyphon-assisted ejector cooling cycle	$\eta_{CS} = \frac{\dot{Q}_{Cooling} + \dot{m}_{57}(h_{58} - h_{57})}{\dot{m}_{44}(h_{44} - h_{45}) + \dot{W}_{P5}}$	$\psi_{CS} = \frac{\dot{E}x^Q_{Cooling} + \dot{m}_{57}(ex_{58} - ex_{57})}{\dot{m}_{44}(ex_{44} - ex_{45}) + \dot{E}x^W_{P5}}$
Drying subsystem	$\eta_{DC} = \frac{\dot{Q}_{Drying}}{\dot{m}_{60}(h_{60} - h_{61})}$	$\psi_{DC} = \frac{\dot{E}x^Q_{Drying}}{\dot{m}_{60}(ex_{60} - ex_{61})}$

Here, V indicates the required electrical potential and is expressed as below [27]:

$$V = V_0 + V_{ohm} + V_{act.a} + V_{act.c} \tag{25}$$

V_0 represents the reversible potential and is calculated by the Nernest equation as following [27]:

$$V_0 = 1.229 + 8.5*10^{-4}(T_{PEM} - 298) \tag{26}$$

In this equation, PEM temperature (T_{PEM}) can be calculated from the local ionic conductivity of the electrolyzer [27]:

$$\sigma_{PEM}[\lambda(X)] = [0.5139\lambda(X) - 0.326]\exp\left[1268\left(\frac{1}{303} - \frac{1}{T_{PEM}}\right)\right] \tag{27}$$

where, x shows the measured depth of membrane from the surface of the cathode membrane, and λ(X) can be calculated as given below [27]:

$$\lambda(X) = \frac{\lambda_a - \lambda_c}{D}x + \lambda_c \tag{28}$$

where, *D* shows the membrane thickness, λ_a and λ_c present membrane anode and cathode surface water.

The ohmic overpotential can be calculated using Ohm's law [25]:

$$V_{ohm} = JR_{PEM} \tag{29}$$

Here, R_{PEM} shows the total resistance of the electrolyzer and can be calculated as [25]:

$$R_{PEM} = \int_0^D \frac{dx}{\sigma_{PEM}[\lambda(X)]} \tag{30}$$

The anode and cathode activation overpotentials are defined as follows [28]:

$$V_{act.i} = \frac{RT}{F}\sinh^{-1}\left(\frac{J}{J_{o.i}}\right) \qquad i = a.c \tag{31}$$

where, $J_{o.i}$ specifies exchange current density, and is computed as [28]:

$$J_{o.i} = J_i^{ref}\exp\left(-\frac{E_{act.i}}{RT}\right) \qquad i = a.c \tag{32}$$

here, J_i^{ref} shows pre-exponential factor, and $E_{act.i}$, presents the activation

Table 5
The energy efficiency for different operating modes of the system.

Various generation	Performance equality
single generation	$\eta_{s-gen} = \frac{(\dot{W}_{Tur} + \dot{W}_{ORC\_T}) - (\sum \dot{W}_P + \sum \dot{W}_{HC} + \sum \dot{W}_{PEM})}{\dot{Q}_{solar}}$
co-generation	$\eta_{c-gen.I} = \frac{(\dot{W}_{Tur} + \dot{W}_{ORC\_T}) - \left(\sum \dot{W}_P + \sum \dot{W}_{HC} + \sum \dot{W}_{PEM}\right) + \dot{Q}_{cooling}}{\dot{Q}_{solar}}$
	$\eta_{c-gen.II} = \frac{(\dot{W}_{Tur} + \dot{W}_{ORC\_T}) - \left(\sum \dot{W}_P + \sum \dot{W}_{HC} + \sum \dot{W}_{PEM}\right) + \dot{Q}_{Heating}}{\dot{Q}_{solar}}$
	$\eta_{c-gen.III} = \frac{(\dot{W}_{Tur} + \dot{W}_{ORC\_T}) - \left(\sum \dot{W}_P + \sum \dot{W}_{HC} + \sum \dot{W}_{PEM}\right) + \dot{m}_{19}LHV_{H_2}}{\dot{Q}_{solar}}$
tri-generation	$\eta_{t-gen.I} = \frac{(\dot{W}_{Tur} + \dot{W}_{ORC\_T}) - \left(\sum \dot{W}_P + \sum \dot{W}_{HC} + \sum \dot{W}_{PEM}\right) + \dot{Q}_{cooling} + \dot{Q}_{Heating}}{\dot{Q}_{solar}}$
	$\eta_{t-gen.II} = \frac{(\dot{W}_{Tur} + \dot{W}_{ORC\_T}) - \left(\sum \dot{W}_P + \sum \dot{W}_{HC} + \sum \dot{W}_{PEM}\right) + \dot{Q}_{cooling} + \dot{m}_{19}LHV_{H_2}}{\dot{Q}_{solar}}$
	$\eta_{t-gen.III} = \frac{(\dot{W}_{Tur} + \dot{W}_{ORC\_T}) - \left(\sum \dot{W}_P + \sum \dot{W}_{HC} + \sum \dot{W}_{PEM}\right) + \dot{Q}_{Heating} + \dot{m}_{19}LHV_{H_2}}{\dot{Q}_{solar}}$
multigeneration	$\eta_{m-gen} = \frac{(\dot{W}_{Tur} + \dot{W}_{ORC_T}) - \left(\sum \dot{W}_P + \sum \dot{W}_{HC} + \sum \dot{W}_{PEM}\right) + \dot{Q}_{cooling} + \dot{Q}_{Heating} + \dot{m}_{19}LHV_{H_2} + \dot{Q}_{fresh\ water} + \dot{Q}_{Drying}}{\dot{Q}_{solar}}$

Table 6
The exergy efficiency for different operating modes of the system.

Various generation	Performance equality
single generation	$\psi_{s-gen} = \frac{(\dot{E}x^{W}_{Tur} + \dot{E}x^{W}_{ORC_T}) - (\sum \dot{E}x^{W}_{P} - \dot{E}x^{W}_{HC} - \dot{E}x^{W}_{PEM})}{\dot{E}x^{Q}_{Solar}}$
co-generation	$\psi_{c\_gen.\ I} = \frac{\left(\dot{E}x^{W}_{Tur} + \dot{E}x^{W}_{ORC_T}\right) - \left(\sum \dot{E}x^{W}_{P} - \dot{E}x^{W}_{HC} - \dot{E}x^{W}_{PEM}\right) + \dot{E}x^{Q}_{Cooling}}{\dot{E}x^{Q}_{Solar}}$
	$\psi_{c\_gen.\ II} = \frac{\left(\dot{E}x^{W}_{Tur} + \dot{E}x^{W}_{ORC_T}\right) - \left(\sum \dot{E}x^{W}_{P} - \dot{E}x^{W}_{HC} - \dot{E}x^{W}_{PEM}\right) + \dot{E}x^{Q}_{Heating}}{\dot{E}x^{Q}_{Solar}}$
	$\psi_{c\_gen.\ III} = \frac{\left(\dot{E}x^{W}_{Tur} + \dot{E}x^{W}_{ORC_T}\right) - \left(\sum \dot{E}x^{W}_{P} - \dot{E}x^{W}_{HC} - \dot{E}x^{W}_{PEM}\right) + \dot{m}_{19} ex^{ch}_{H_2}}{\dot{E}x^{Q}_{Solar}}$
tri-generation	$\psi_{t\_gen.\ I} = \frac{\left(\dot{E}x^{W}_{Tur} + \dot{E}x^{W}_{ORC_T}\right) - \left(\sum \dot{E}x^{W}_{P} - \dot{E}x^{W}_{HC} - \dot{E}x^{W}_{PEM}\right) + \dot{E}x^{Q}_{Cooling} + \dot{E}x^{Q}_{Heating}}{\dot{E}x^{Q}_{Solar}}$
	$\psi_{t\_gen.\ II} = \frac{\left(\dot{E}x^{W}_{Tur} + \dot{E}x^{W}_{ORC_T}\right) - \left(\sum \dot{E}x^{W}_{P} - \dot{E}x^{W}_{HC} - \dot{E}x^{W}_{PEM}\right) + \dot{E}x^{Q}_{Cooling} + \dot{m}_{19} ex^{ch}_{H_2}}{\dot{E}x^{Q}_{Solar}}$
	$\psi_{t\_gen.\ III} = \frac{\left(\dot{E}x^{W}_{Tur} + \dot{E}x^{W}_{ORC_T}\right) - \left(\sum \dot{E}x^{W}_{P} - \dot{E}x^{W}_{HC} - \dot{E}x^{W}_{PEM}\right) + \dot{E}x^{Q}_{Heating} + \dot{m}_{19} ex^{ch}_{H_2}}{\dot{E}x^{Q}_{Solar}}$
multigeneration	$\psi_{m\_gen} = \frac{\left(\dot{E}x^{W}_{Tur} + \dot{E}x^{W}_{ORC_T}\right) - \left(\sum \dot{E}x^{W}_{P} - \dot{E}x^{W}_{HC} - \dot{E}x^{W}_{PEM}\right) + \dot{E}x^{Q}_{Cooling} + \dot{E}x^{Q}_{Heating} + \dot{E}x^{Q}_{Drying} + \dot{E}x^{Q}_{freshwater} + \dot{m}_{19} ex^{ch}_{H_2}}{\dot{E}x^{Q}_{Solar}}$

Table 7
Comparison of the calculated results for the system in present study and Ref. [10].

Hydrogen production rate (kg/hr)	Exergy efficiency (%)	Subsystem with the most damage	Amount of Duty Power generated (kW)	
15.48	56.51	Solar Subplant	3545	**Ref.** [10]
15.48	58.04	Solar Subplant	3545	**Current study**

energy.

Necessary input parameters for PEM electrolyzer modeling are listed in Table 3.

3.4. Energy and exergy evaluation of the system

Energy efficiency is rate of system energy products to its input rate. Similarly, the exergy efficiency is the ratio of the products' exergy rate to that of the input stream. The energy and exergy efficiency terms of each subsystem in the multigeneration system are given in Table 4.

Moreover, the energy and exergy efficiencies for single, co, tri, and multigeneration cases of the proposed system are defined in Table 5 and 6. In the single generation system, only electricity generation is considered. Cogeneration systems have been studied in three ways: combining electricity and cooling (cogeneration I), electricity and heating (cogeneration II), electricity and hydrogen (cogeneration III) cogeneration cases. The trigeneration systems are: electricity-cooling-heating (trigeneration I), electricity-cooling-hydrogen (trigeneration II), and electricity-heating-hydrogen (trigeneration III) trigeneration systems. Finally, the multigeneration system includes all products, i.e., electricity, cooling, heating, drying air, freshwater, and hydrogen.

3.5. Environmental and exergoeconomic evaluation of the system

To improve environmental sustainability, not only sustainable renewable energy sources should be considered, but also nonrenewable sources should be used in such a way that their negative impacts become as low as possible. Hence, the stability index can relate the exergy efficiency to the environmental performance as following [22,29].

$$SI = \frac{1}{1-\psi} \tag{29}$$

Exergoeconomic factor is an important parameter for the choice of

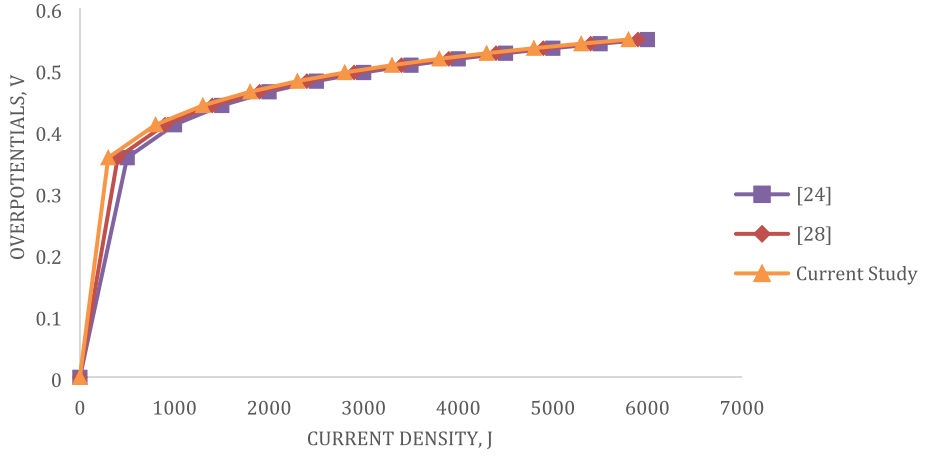

Fig. 3. Validation result of PEM hydrogen production unit in this work with Refs. [24,28].

Table 8
Thermodynamic and exergoeconomic properties of the system state points.

State	Working fluid	$\dot{m}$(kg/s)	T (°C)	P (Kpa)	(Kj/Kg) h	(Kj/Kgmol-C)s	(Kj/Kg)ex	c ($/GJ)
1	Therminol 66	25	325	2500	576.4	0.0542	4845.54	137.73
2	Therminol 66	25	302	2500	517.2	0.155	48426.4	137.84
3	Therminol 66	25	303.2	2500	517.8	0.1541	48426.7	138.03
4	Therminol 66	25	269	101.3	433.6	0.2988	48385.7	138.03
5	Therminol 66	25	242	2460	370.6	0.4239	48360	138.03
6	Therminol 66	25	203	2460	282.1	0.6025	48324.7	138.03
7	Therminol 66	25	190	2460	252.9	0.6646	48314	138.03
8	Therminol 66	25	90.41	2460	54.33	1.146	4825.88	138.03
9	Therminol 66	25	84	2440	42.83	1.177	4825.88	138.03
10	Therminol 66	25	73	110	21.17	1.231	4825.13	138.07
11	Therminol 66	25	73.24	2500	24.01	1.231	4825.06	138.23
12	Sea water	10	25	101.3	15150	8.661	52.14	0
13	Brine	0.88	40	101.3	7730	4.916	3.241	10760.3
14	Water	9.28	40	101.3	15800	8.855	1.525	10760.3
15	Water	9.28	28.75	101.3	15870	3.035	49.91	10760.3
16	Water	7.1	28.75	101.3	15870	3.035	49.91	10760.3
17	Water	7.1	80	101.3	15650	3.714	69.57	492.55
18	Oxygen	0.0021	80	101.3	15650	3.714	0	15979
19	Hydrogen	0.0043	80	101.3	2559	11.61	326679.7	15979
20	Hydrogen	0.0043	640.4	500	1197	12.87	326776.4	15975.2
21	Hydrogen	0.0043	361.1	500	1894	11.96	32673.8	15975.2
22	Hydrogen	0.0043	640.1	1500	1197	12.16	32679.7	15972.5
23	Hydrogen	0.0043	150	1500	1986	7.1	32673.6	15972.5
24	Hydrogen	0.0043	235.1	2500	2201	10.38	326751.6	15971.9
25	Hydrogen	0.0043	80	2500	2967	8.496	326730.3	15971.9
26	Water	0.0161	29	110	15870	3.039	50.09	0
27	Water	0.0161	72	110	15680	3.614	64.48	0.04065
28	Water	0.0332	29	110	15870	3.039	50	0
29	Water	0.0332	72	110	15680	3.614	64.51	32218.9
30	Water	0.0771	29	110	15870	3.039	50	0
31	Water	0.0771	72	110	15680	3.614	64.51	50568472
32	Ammonia- water	53.17	94.21	1917	8428	5.769	201398.7	0.4667
33	Ammonia- water	12.75	94.21	1917	2827	8.977	32991.7	0.12
34	Ammonia- water	12.75	165	1917	2653	9.409	329961.5	0
35	Ammonia- water	12.75	67.75	510.8	2847	9.526	329732.4	0
36	Ammonia- water	40.42	94.21	1917	10190	4/757	159800.6	0
37	Ammonia- water	40.42	53.67	510.8	10190	4.810	159785	0
38	Ammonia- water	53.17	54.63	510.8	8432	5.941	201342.4	0
39	Ammonia- water	53.17	51.48	510.8	8477	5.803	201338.5	0
40	Ammonia- water	53.17	93.36	1917	8441	5.731	201396.1	0.4603
41	Water	20.34	20	110	15910	2.908	50.16	0
42	Water	21.34	46	110	15800	3.275	53	17.935
43	R113	27.22	179.3	2000	3621	3.192	5706.6	223.152
44	R113	27.22	98.5	83.86	3660	3.219	5659.3	223.152
45	R113	27.22	40.88	83.86	3805	2.769	5648.7	223.152
46	R113	27.22	85	2000	3803	2.762	5652.48	223.848
47	Isobutane	10.19	95.5	1821	2238	2.645	48357.9	5467.84
48	Isobutane	10.19	43.9	488	2297	2.622	4828.96	5467.86
49	Isobutane	10.19	37	488	2628	1.556	48292.6	5467.86
50	Isobutane	10.19	37	488	2628	1.556	48292.6	5467.86
51	Isobutane	10.19	6.948	198	2628	1.571	48288.2	5467.86
52	Isobutane	10.19	6.948	198	2352	2.558	48270.4	5467.86
53	Isobutane	10.19	37	488	2628	1.556	48292.6	5467.86
54	Isobutane	10.19	38.26	1821	2625	1.559	48295	5478.78
55	Water	46.62	22	102	15900	2.937	50	0
56	Water	46.62	8	102	15960	2.728	52.14	407.694
57	Water	72.70	18	110	15920	2.879	50.33	0
58	Water	72.70	39.5	110	15830	3.186	51.44	393.374
59	Air	45.20	28	150	416/0	3.969	1748.6	0
60	Air	45.20	80	150	48/54	4.138	1753.1	0.08724
61	Water	46.62	8.105	102	15960	2.729	52.1	407.694
62	Air	118	20	200	5.524	3.869	1773.1	0
63	Air	118	9	200	16.44	3.831	1773.5	0.00247
64	Methanol	0.016	22	12.02	6287	4.789	5.73	–
65	Methanol	0.016	9	12.02	7605	0.3213	5.73	–

design parameters. This factor represents the share of capital and maintenance costs (non-exergy costs) in the component total cost. Therefore, its low value indicates the need for a more cost-effective redesign, which can be achieved by increasing the exergy efficiency and reducing the exergy destruction of that component. On the other hand, its high value signifies a reduction in the component capital expenditure. This parameter can be calculated as below [29]:

$$f_k = \frac{\dot{Z}_k}{\dot{Z}_k + c_{F,k}\left(\dot{E}_{D,k} + \dot{E}_{L,k}\right)} \tag{30}$$

Also, a component cost different ratio can be determined as [29]:

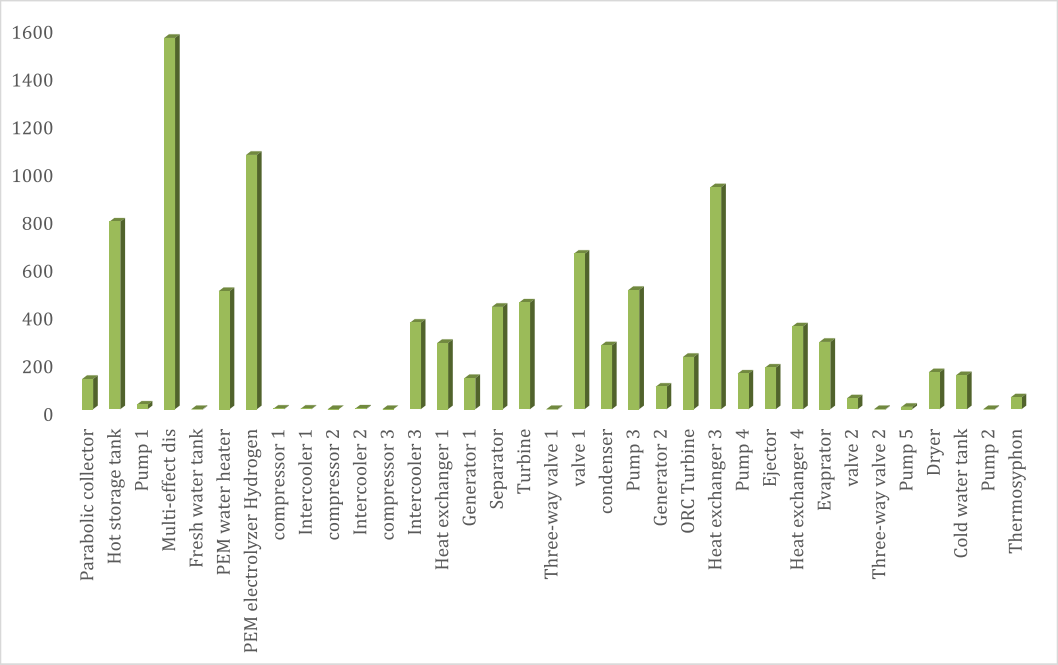

Fig. 4. Exergy destruction rate of the system components.

Table 9
Thermodynamic evaluation results of the system.

Subsystem	Energy efficiency (%)	Exergy efficiency (%)	Sustainability index	Exergy destruction rate (Kw)
Parabolic collector system	39.28	35.32	1.54	5195.9
Freshwater production	55.71	45.46	1.83	1553.59
Hydrogen generation and compression	14.37	11.17	1.12	1910.87
Kalina cycle	50.19	47.84	1.91	3671.49
Organic Rankine Cycle	46.82	43.67	1.77	358.87
Cooling subsystem	74.15	70.26	3.36	707.66
Dryer	78.65	71.17	3.46	154.4
The multigeneration system	61.34	58.04	2.38	13552.7

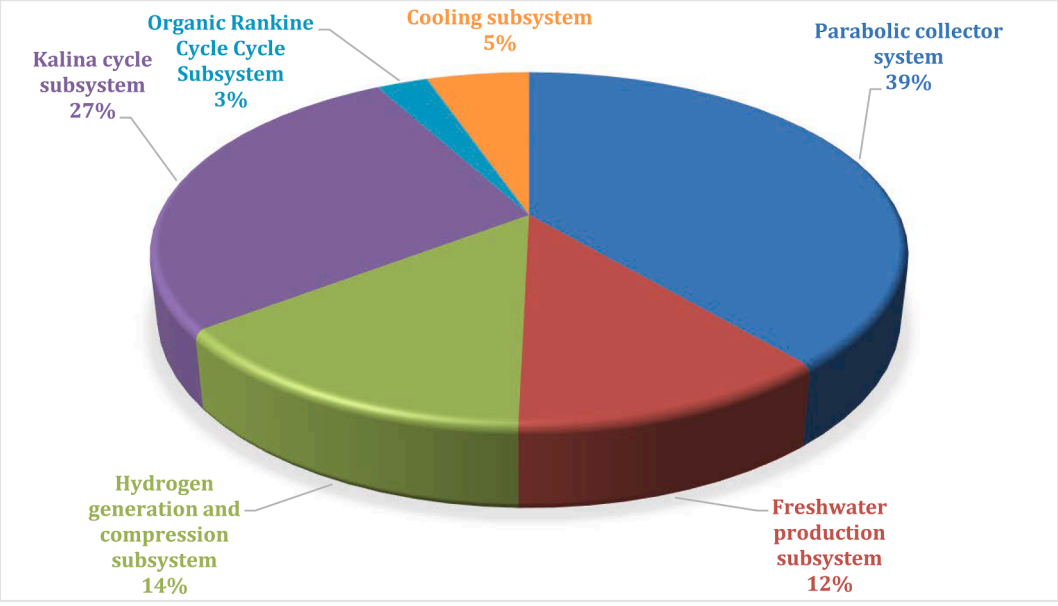

Fig. 5. Contribution of different units of the proposed system to the total exergy destruction.

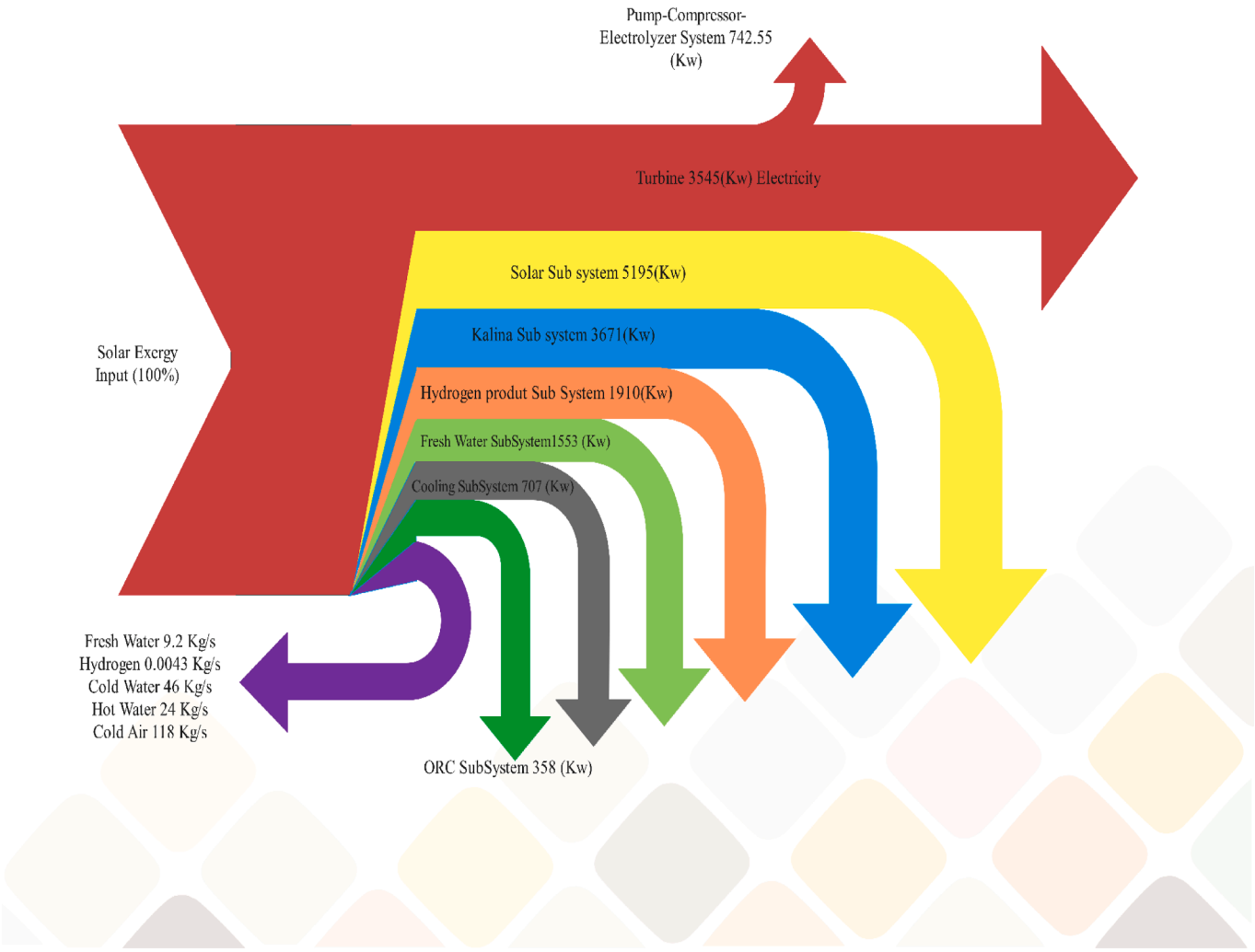

Fig. 6. Grassmann-Sankey diagram for the proposed multigeneration system.

$$r_k = \frac{c_{P.k} - c_{F.k}}{c_{F.k}} \tag{31}$$

4. Results and discussion

In this section, the results of thermodynamic and exergoeconomic modeling of the system using Aspen HYSYS software are reported and discussed.

Table 7 compares the results obtained from the present study to those of ref. [10] and shows a good agreement between them with a relative error of about 2.71%.

Fig. 3 compares the hydrogen production rate in the PEM obtained from the present study to those of ref. [24,28] and shows a good agreement between them with an error of less than 1%.

Table 8 lists thermodynamic and exergoeconomic properties of the streams in the multigeneration system.

Fig. 4 shows the exergy destruction rate of the system equipment. According to this figure, the multi-effect distillation unit with 1553.59 kW and the proton exchange membrane electrolyser with 1064.26 kW have the highest exergy destruction rates, since these two components consume electrical power to perform the desired separations, i.e., fresh water from brine in the seawater desalination unit and hydrogen from oxygen in the PEM water electrolyzer unit.

Table 9 contains the thermodynamic results, i.e., energy and exergy efficiencies, sustainability index, and exergy destruction rate for the subsystems and the overall system. As evident, air dryer is the most efficient unit, both from energy and exergy aspects; its energy and exergy efficiencies are 78.65% and 71.17%, respectively. It also has the highest sustainability index, which is 3.46. This is due to its simplicity in design and performance. On the other hand, the energy and exergy efficiencies of the proposed multigeneration system are 61.34% and 58.04%, respectively, and its sustainability index is calculated as 2.38. Furthermore, total exergy destruction rate of the system is obtained as 13552.7 kW.

Fig. 5 shows the contribution of each subsystem to the total exergy destruction, and it can be seen that the highest exergy destruction ratios belong to the solar parabolic collection subsystem, 39%, and Kalina cycle, 27%. Additionally, the organic Rankine cycle has the lowest contribution to the total exergy destruction rate.

Fig. 6 is known as the Grossman-Sanki diagram, and can be used to illustrate the amount of total input exergy, the locations of exergy destruction, and the amount of net exergy output for each subsystem. According to this diagram, 41.96% of the total energy entering the system, has been wasted and destroyed in various ways in the system by the equipment and converters used in the combined system.

Thermodynamic results of different hybrid systems, i.e., single/co/trigeneration cases, are shown in Fig. 7. As obvious in this figure, the more the number of output products, the higher the energy and exergy efficiencies. For instance, in single generation case, the energy and exergy efficiencies are 28% and 26.11%, respectively. However, if cogeneration scheme is considered, the energy efficiency increases at least to 35.5% and the exergy efficiency to 33.51%. Also, they increase

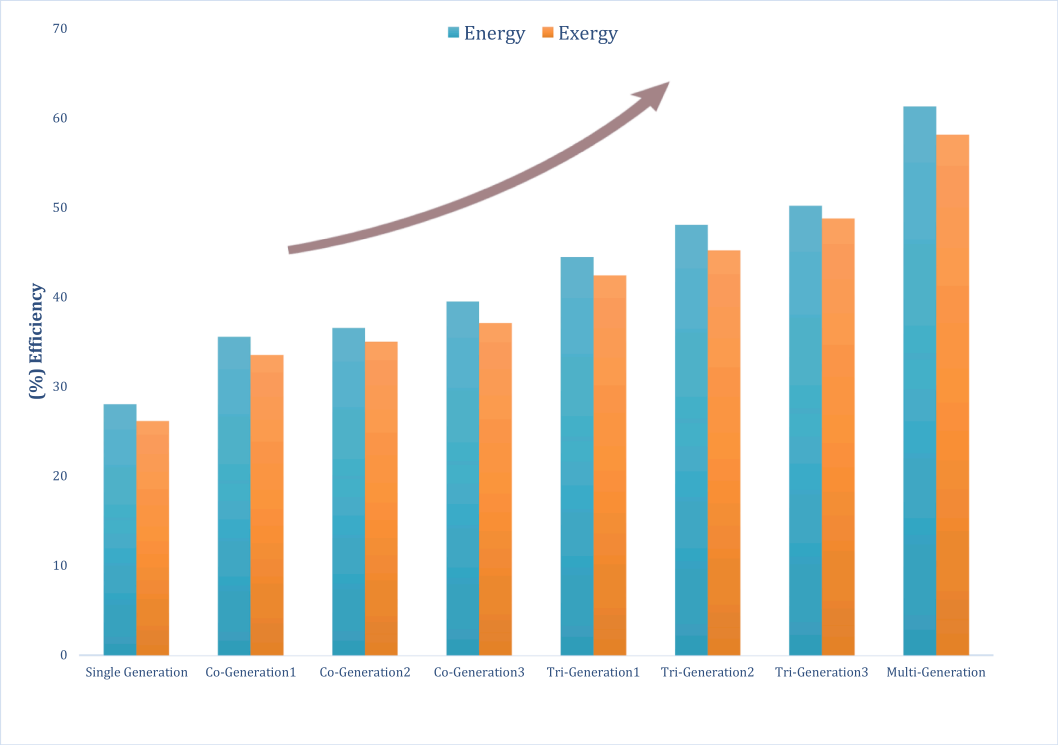

Fig. 7. Energy and exergy efficiencies of different operation scenarios of the proposed system.

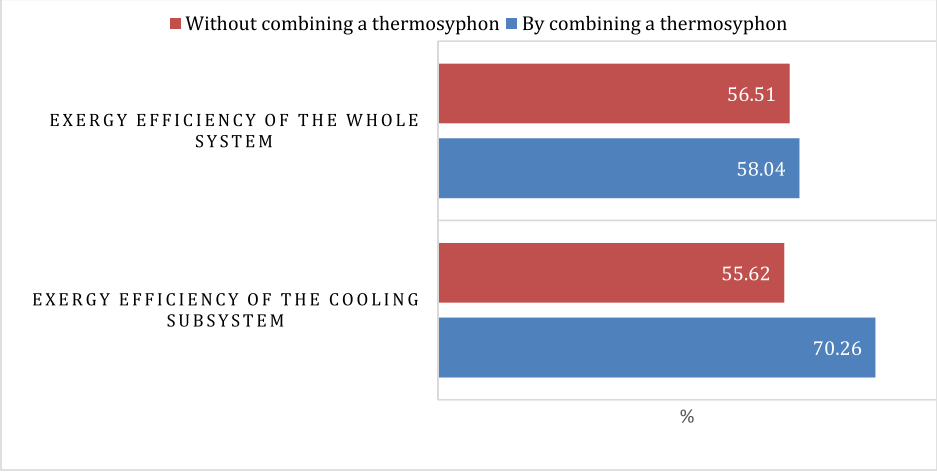

Fig. 8. The effect of thermosyphon on the exergy efficiency.

to 61.2% and 58.05%, respectively for the multi-generation scenario. This proves the advantages of recovering waste heat and material from a thermodynamic system as an input resource for other bottoming cycles leading to higher efficiencies and lower cost.

Fig. 8 shows the effect of adding a thermosyphon to the ejector cooling system on the exergy efficiency. In this case, the exergy efficiency of this unit increases from 55.62% to 70.27% due to the fact that a thermosyphon system has natural fluid circulation without the need for energy consumption. Furthermore, the exergy efficiency of the whole system is improved by 2.71% compared to the reference system [10]. The reason can be attributed to the effect of the integration of the thermosyphon subsystem to the reference system.

The results of economic analysis for the proposed system are obtained by transferring thermodynamic data through Excel to EES and solving the related exergoeconomic equations as a cost matrix (shown in Appendix A) in EES software.

The exergoeconomic results of the subsystems and multigeneration system are summarized in Table 10. According to this table, the PEM electrolyzer with 903.62, freshwater storage with 1.2058, pump3 with 1.138, and separator with 0.449 have the highest cost difference ratios, respectively. Also, the highest cost rate belongs to the electrolyzer and organic Rankine cycle turbine with 9288354.7$ and 2188252.7$, respectively, meaning that the largest part of the investment cost is paid to these components and special attention should be paid to decreasing their prices. Furthermore, the Kalina turbine, freshwater storage tank, valve1, condenser, and pump3 own the highest exergoeconomic factor, implying that their capital cost is too high and should be reduced even if it leads to their increased exergy destruction.

Fig. 9 shows the contribution of each equipment to the cost destruction of the system. As evident in this figure, the highest cost

Table 10
Exergoeconomic results of the system.

Equipment name	Cost ($)	cost destruction rate ($ / h)	Cost difference ratio	Exergoeconomic factor
Parabolic collector	98750	355.5	0.00059	0.0013
Hot storage tank	23976.71	86.316	0.000143	0
Pump1	40304.76	145.09	0.00146	0.0035
Multi-effect distillation unit	–	26.715	0	0
Freshwater storage tank	38967.077	662.87	1.2058	1
PEM water heater	503.6785	13230.83	0.02151	0
PEM electrolyzer Hydrogen	9288354.7	893.25	903.62	0.907
compressor1	6.841	48.798	0	0
Intercooler1	20289.83	103.51	0.000128	0.0154
compressor2	116.9	24.959	0	0.00056
Intercooler2	20289.83	73.043	0	0.0120
compressor3	2.073	7.164	0	0
Intercooler3	20289.83	73.043	0	0
Heat exchanger1	388408.75	2272.88	0.00377	0.0023
Generator1	31430.294	113.149	0.00018	0.00039
Separator	–	8078.69	0.449	0
Kalina Turbine	1424471.72	0	0.0006	1
Three-way valve1	–	0	0.0043	0
valve1	90.95	0	0	1
Condenser	20290.2	0	0	1
Pump3	475088	0	1.138	1
Generator2	31430.29	685.77	0.00114	0.00055
Organic Rankine Cycle Turbine	2188252.7	1035.51	0.0082	0.074
Heat exchanger3	20289.83	73.04	0	0
Pump4	23894.17	467.95	0.0037	0.0013
Ejector	2506504	9023.4	0.00046	0.00074
Heat exchanger4	20289.83	73.043	0	0
Evaporator	204899.12	0	0	0
valve2	68.33	886.92	0	0
Three-way valve2	–	0	0	0
Pump5	18749.16	349.56	0	0.0002
Dryer	2423	0.0406	0	0
Cold water storage tank	23976.7	86.31	0.0001	0.00038
Pump2	33941.4	714.48	0.00119	1
Thermosyphon	0	143.78	0.03342	0.0013

destruction occurs in the heat exchanger of the proton exchange membrane (33.29%), ejector (22.7%), and separator (20.33%), respectively. Therefore, these three devices impose the highest cost on the system according to the obtained economic results.

5. Conclusion

In these cycles, units have been integrated so that maximum energy and material recovery are achieved to enhance the system efficiency and decrease waste. Mass and energy conservation laws along with exergy and thermoeconomic relations are applied to each piece of equipment at steady state zero-dimensional conditions. Aspen HYSYS and EES are used to simulate the energy, exergy, and exergoeconomic performances of the system. The obtained results can be summarized as follows:

- Energy and exergy efficiency of the proposed multigeneration system are 61.34% and 58.08%, respectively.
- The sustainability index of the system is 2.38 which shows that it has good environmental performance.
- Kalina cycle has the highest share in the total amount of energy production with 2457 kW power generation.
- The dryer unit has the best thermodynamic efficiency and the highest sustainability index with 78.65% and 3.46, respectively.
- Integration of the thermosyphon into the refrigeration unit increases the exergy efficiency from 55.62% to 70.26%.
- Water heater of the proton exchange membrane, ejector, and Kalina cycle separator own the highest cost destruction rates with 33.3%, 22.7%, and 20.33%, respectively.
- Parabolic collector system with 39%, has the highest exergy destruction ratio.

The following ideas may be taken into account as the next steps of this work:

- Biofuel, wind, and other renewable energy sources, among others, can be employed instead of solar energy, and their effects on the system can all be investigated.
- The effect on the system operation of changing some main parameters such as solar radiation intensity, pressure ratio, generator temperature, pump pressure, and Kalina cycle ammonia concentration can be studied comprehensively.

It should also be mentioned that along with the advantages of these systems, one should pay attention to the challenges in making them practical. The challenges that may be related to the practical application of the system are: dependence on solar energy, predictable and unpredictable changes that will lead to the instability of the energy system (day and night, seasonal changes or cloudiness of the air), the relatively high investment cost compared to the use of fossil fuels (not in all cases) and integrated systems, complex maintenance, repair, control, and optimization of the process.

Declaration of Competing Interest

The authors declare that they have no known competing financial interests or personal relationships that could have appeared to influence the work reported in this paper.

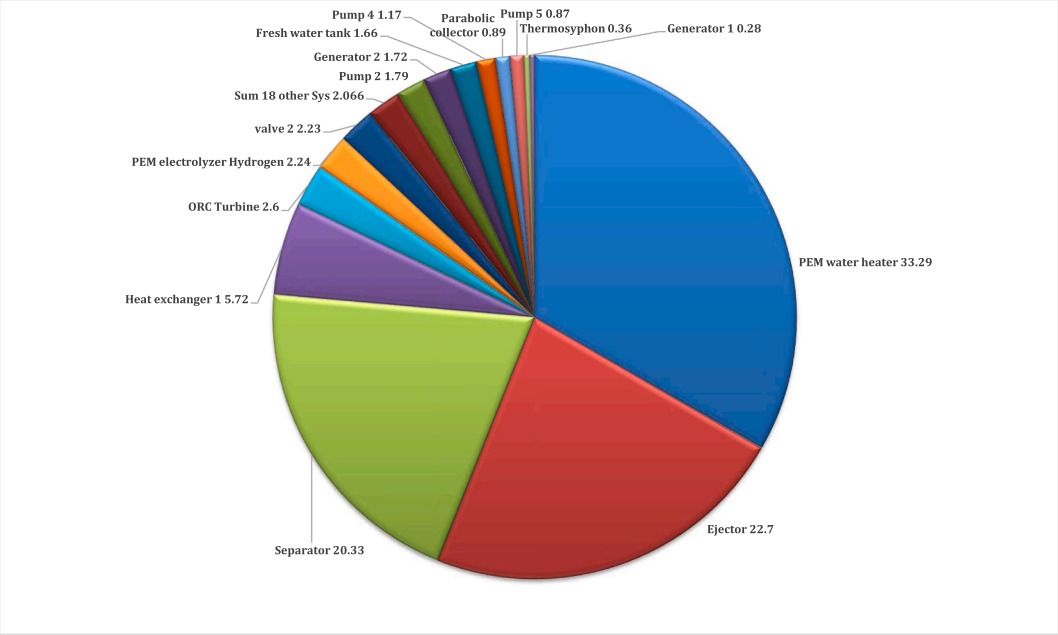

Fig. 9. Contribution of each equipment to the cost destruction ratio.

Appendix A. Exergoeconomic analysis equation matrix

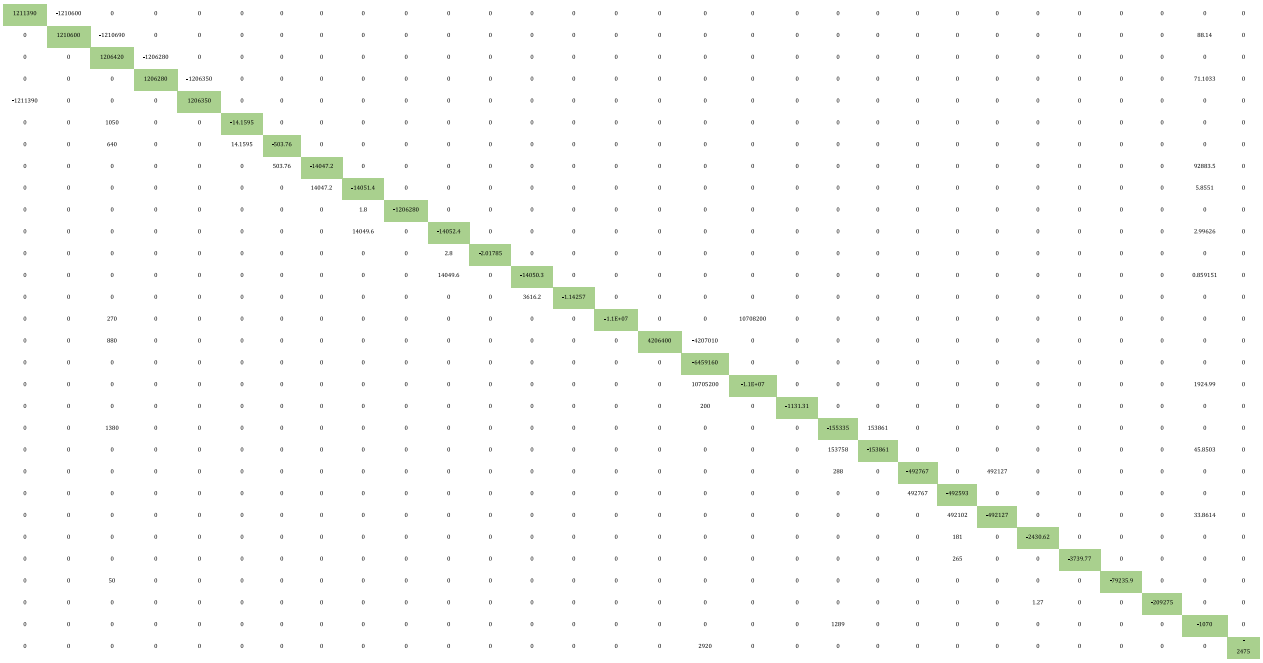

References

[1] BP, Statistical Review of World Energy 2020 | 69th edition.

[2] Roy, J., Mishra, M., Misra, A., 2010. Parametric optimization and performance analysis of a waste heat recovery system using Organic Rankine Cycle. Energy 35, 5049–5062.

[3] M.R. Patel, Wind and solar power systems: design, analysis, and operation, CRC press2005.

[4] Kotas, T., 1995. The Exergy Analysis Method of Thermal Plant Analysis. Krieger, Melbourne, Australia.

[5] Ahmadi, P., Dincer, I., Rosen, M.A., 2012. Exergo-environmental analysis of an integrated organic Rankine cycle for trigeneration. Energ. Conver. Manage. 64, 447–453.

[6] Ozturk, M., Dincer, I., 2013. Thermodynamic analysis of a solar-based multi-generation system with hydrogen production. Appl. Therm. Eng. 51, 1235–1244.

[7] Leiva-Illanes, R., Escobar, R., Cardemil, J.M., Alarcón-Padilla, D.-C., Uche, J., Martínez, A., 2019. Exergy cost assessment of CSP driven multi-generation schemes: Integrating seawater desalination, refrigeration, and process heat plants. Energ. Conver. Manage. 179, 249–269.

[8] Chen, Y., Xu, D., Chen, Z., Gao, X., Han, W., 2019. Energetic and exergetic analysis of a solar-assisted combined power and cooling (SCPC) system with two different cooling temperature levels. Energ. Conver. Manage. 182, 497–507.

[9] Sezer, N., Koç, M., 2019. Development and performance assessment of a new integrated solar, wind, and osmotic power system for multigeneration, based on thermodynamic principles. Energ. Conver. Manage. 188, 94–111.
[10] Tukenmez, N., Koc, M., Ozturk, M., 2020. Development and performance analysis of a concentrating collector combined plant for multigeneration purposes. Energ. Conver. Manage. 205, 112415.
[11] Demir, M.E., Dincer, I., 2018. Development and analysis of a new integrated solar energy system with thermal storage for fresh water and power production. Int. J. Energy Res. 42, 2864–2874.
[12] He, T., Mei, C., Longtin, J.P., 2017. Thermosyphon-assisted cooling system for refrigeration applications. Int. J. Refrig. 74, 165–176.
[13] Casallas, C., Dincer, I., 2017. Assessment of an integrated solar hydrogen system for electrochemical synthesis of ammonia. Int. J. Hydrogen Energy 42, 21495–21500.
[14] Hosseinnia, H., Mohammadi-Ivatloo, B., Mohammadpourfard, M., 2022. Multi-objective configuration of an intelligent parking lot and combined hydrogen, heat and power (IPL-CHHP) based microgrid. Sustain. Cities Soc. 76, 103433.
[15] Elsheikh, A.H., Panchal, H.N., Sengottain, S., A. Alsaleh, N., Ahmadein, M., 2022. Applications of Heat Exchanger in Solar Desalination: Current Issues and Future Challenges. Water. 14 (6), 852.
[16] Nabat, M.H., Soltani, M., Razmi, A.R., Nathwani, J., Dusseault, M.B., 2021. Investigation of a green energy storage system based on liquid air energy storage (LAES) and high-temperature concentrated solar power (CSP): Energy, exergy, economic, and environmental (4E) assessments, along with a case study for San Diego. US. Sustainable Cities and Society. 75, 103305.
[17] Elsheikh, A.H., El-Said, E.M.S., Abd Elaziz, M., Fujii, M., El-Tahan, H.R., 2023. 135896. ISSN 388, 135896.
[18] Bieliski, H., Mikielewicz, J., 2011. Heat Transfer - Mathematical Modelling, Numerical Methods and Information Technology. InTech.
[19] Kalogirou, S., 2003. The potential of solar industrial process heat applications. Appl. Energy 76 (4), 337–361.
[20] Sorgulu, F., Dincer, I., 2019. Design and analysis of a solar tower power plant integrated with thermal energy storage system for cogeneration. Int J Energy Res 43 (12), 6151–6160.
[21] Sakthivel, P., Anandha babu, G., Karuppiah, M., Asaithambi, S., Balaji, V., Pandian, M.S., Ramasamy, P., Mohammed, M.K.A., Navaneethan, N., Ravi, G., 2022. Electrochemical energy storage applications of carbon nanotube supported heterogeneous metal sulfide electrodes. Ceram. Int. 48 (5), 6157–6165.
[22] Bejan, A., Tsatsaronis, G., Moran, M., 1996. Thermal Design and Optimization John Wiley and Sons. Inc, New York.
[23] Dincer, I., Rosen, M.A., 2012. Exergy: energy, environment and sustainable development. Elsevier Science.
[24] P. Ahmadi, Modeling, analysis and optimization of integrated energy systems for multigeneration purposes, 2013.
[25] Abam, F.I., Briggs, T.A., Diemuodeke, O.E., Ekwe, E.B., Ujoatuonu, K.N., Isaac, J., Ndukwu, M.C., 2020. Thermodynamic and economic analysis of a Kalina system with integrated lithium-bromide-absorption cycle for power and cooling production. Energy Rep. 6, 1992–2005.
[26] Kumar, A., Singh, S., Mohammed, M.K.A., Esmail Shalan, A., 2021. Effect of 2D perovskite layer and multivalent defect on the performance of 3D/2D bilayered perovskite solar cells through computational simulation studies. Sol. Energy 223, 193–201.
[27] AlZahrani, A.A., Dincer, I., 2016. Design and analysis of a solar tower based integrated system using high temperature electrolyzer for hydrogen production. Int. J. Hydrogen Energy 41 (19), 8042–8056.
[28] Ni, M., Leung, M.K., Leung, D.Y., 2008. Energy and exergy analysis of hydrogen production by a proton exchange membrane (PEM) electrolyzer plant. Energ. Conver. Manage. 49, 2748–2756.
[29] Ghaebi, H., Saidi, M., Ahmadi, P., 2012. Exergoeconomic optimization of a trigeneration system for heating, cooling and power production purpose based on TRR method and using evolutionary algorithm. Appl. Therm. Eng. 36, 113–125.